Expert Systems With Applications 240 (2024) 122585

Contents lists available at ScienceDirect

Expert Systems With Applications

journal homepage: www.elsevier.com/locate/eswa

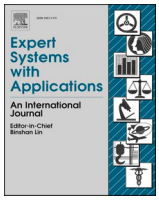

Machine learning-based radiomics for amyotrophic lateral sclerosis diagnosis

Benedetta Tafuri [a,b,*], Giammarco Milella [a,b], Marco Filardi [a,b], Alessia Giugno [b,d], Stefano Zoccolella [b,c], Ludovica Tamburrino [a,b], Valentina Gnoni [b], Daniele Urso [b], Roberto De Blasi [b], Salvatore Nigro [b,1], Giancarlo Logroscino [a,b,1]

[a] Department of Translational Biomedicine and Neuroscience (DiBraiN), University of Bari Aldo Moro, Bari, Italy
[b] Center for Neurodegenerative Diseases and the Aging Brain, University of Bari Aldo Moro at Pia Fondazione "Card. G. Panico", Tricase, Italy
[c] Neurology Unit, San Paolo Hospital, Azienda Sanitaria Locale (ASL) Bari, Bari, Italy
[d] Department of Medical and Surgical Sciences, Institute of Neurology, Magna Graecia University, Catanzaro, Italy

ARTICLE INFO

Keywords:
Amyotrophic lateral sclerosis
Magnetic resonance imaging
Radiomics
Machine learning

ABSTRACT

Timely diagnosis and accurate phenotyping of amyotrophic lateral sclerosis (ALS) is of paramount importance for the clinical management of patients. Magnetic Resonance Imaging (MRI) plays a key role in the clinical work-up of ALS. In this study we investigated the usefulness of radiomics analysis on T1-weighted MRI to define a machine learning-based classification pipeline.

We collected 53 controls and 84 patients with ALS from three different scanners. Following dataset harmonization, radiomics analysis was conducted using different features selection and machine learning algorithms to identify the best combination in distinguishing ALS patients from controls and "Classic" from "non-Classical" ALS motor phenotypes.

The combined Least Absolute Shrinkage and Selection Operator with Support Vector Machine (SVM) algorithm classified ALS patients with an accuracy of 81.1%. The Maximum Relevance Minimum Redundancy with SVM pipeline was able to distinguish "Classic" from "non-Classical" motor phenotypes with 92.9% accuracy.

Radiomics is a promising approach to characterize brain abnormalities in patients with ALS. Radiomics could help to improve diagnosis and may prove useful to assess disease severity and longitudinally monitor ALS patients along the disease course.

1. Introduction

Amyotrophic lateral sclerosis (ALS) is a fatal neurodegenerative disease showing a progressive degeneration of motor neurons in the cortex, brainstem and spinal cord (Kiernan et al., 2011). Although first described over 150 years ago, the diagnostic landscape for ALS remains complex. Therefore, various diagnostic criteria for ALS have been proposed over time: while some emphasize clinical evaluations of upper motor neuron (UMN) and lower motor neuron (LMN) signs (Brooks, 1994; Brooks et al., 2000; Hannaford et al., 2021), others incorporate neurophysiological or instrumental exams for increased diagnostic precision (de Carvalho et al., 2008). Achieving an early diagnosis is critical as it allows timely intervention and facilitates patient enrollment in clinical trials. Thanks to the introduction of new classification systems and through many population-based studies, the understanding of ALS epidemiology has progressively advanced. For instance, the EURALS consortium, which collected data from nearly 24 million individuals across Europe, reported an ALS incidence of 2.2 per 100,000 person-years. In contrast, studies have found the lowest incidences in East Asia and South Asia, at 0.89 and 0.79 per 100,000 person-years, respectively (Logroscino & Piccininni, 2019).

Simultaneous degeneration of UMN and LMN not only represents a hallmark of the diagnosis of ALS disease but also explains the extreme phenotypic heterogeneity among ALS patients. In this context, over the past years, several classification systems have been proposed among which the one developed by Chiò et al. in 2011 recognizes six different phenotypes, namely "Classical" ALS, bulbar ALS, respiratory ALS, flail arm ALS, pyramidal ALS, and flail leg ALS (Chiò et al., 2011). These

* Corresponding author at: Department of Translational Biomedicine and Neuroscience (DiBraiN), University of Bari Aldo Moro, Bari, Italy.
E-mail addresses: benedetta.tafuri@uniba.it (B. Tafuri), giancarlo.logroscino@uniba.it (G. Logroscino).
[1] These authors contributed equally and share last authorship.

https://doi.org/10.1016/j.eswa.2023.122585
Received 4 September 2023; Received in revised form 13 November 2023; Accepted 13 November 2023
Available online 14 November 2023

nosological entities are associated with different anatomical areas of motor neuron involvement and clinical course. "Classical" ALS involves simultaneous UMN and LMN degeneration and is usually fatal within 4 years from disease onset. Conversely, the "non-Classical" ALS phenotypes are associated with longer survival and report predominant and more specific onset of symptoms (Schito et al., 2020).

Therefore, the correct and timely identification of "Classical" ALS phenotype is of utmost importance to personalize therapeutic approaches (Miller et al., 2009) and to stratify new patients for possible enrolment in clinical trials (Hardiman et al., 2011). The classification system of Chio et al. relies on data collected during the first year of illness, allowing the disease's symptoms to manifest more clearly and enabling the clinician to assess the progression rate more accurately. Accordingly, there is a great deal of interest among clinicians and researchers in the field of ALS, in identifying reliable biomarkers able to distinguish the different ALS phenotypes as earlier as possible, ideally at the time of diagnosis.

Magnetic Resonance Imaging (MRI) has progressively acquired greater relevance for the *in vivo* assessment of central nervous system damage in ALS patients. Previous MRI studies revealed several imaging features associated to the development of ALS, including degeneration of the basal ganglia and brainstem structures (Milella et al., 2022), precentral gyrus (Bede et al., 2013; Schuster et al., 2014), corpus callosum (Schuster et al., 2016) and corticospinal tracts (CST) (Ciccarelli et al., 2009). Cluster-based and supervised prediction models based on imaging biomarkers have been also developed and evaluated in many studies (Bede et al., 2017; Ferraro et al., 2017; Fratello et al., 2017; Grollemund et al., 2019; Rajagopalan et al., 2023; Schuster et al., 2016; Thome et al., 2022; Welsh et al., 2013). Nonetheless, these approaches achieved suboptimal discriminative performances with accuracy ranging from 59 %, for volumetric studies, to 89 % for combined models (i.e., clinical and diffusion-based imaging features).

In the context of non-invasive classification of ALS, radiomics represents a novel approach that extrapolates from conventional MRI images a higher number of quantitative data. Radiomics combines traditional radiology, big data analysis and machine learning approaches to fill the gap between qualitative and quantitative radiology and pattern-based information from radiomics analysis. Radiomic has been successfully used in the field of neurodegenerative diseases showing excellent performances for both classification (Cheung et al., 2022; Salmanpour et al., 2023; Salvatore et al., 2019; Tafuri, Filardi, et al., 2022) and prognostic goals (Jain et al., 2021; Tafuri et al., 2023).

In the current study, we explored the predictive power of radiomics on structural T1-weighted MR images in differentiating ALS patients from healthy controls. Moreover, we assessed whether radiomics-based analysis could distinguish "Classical" from "non-Classical" ALS phenotypes, as the former is the most common ALS phenotype, associated with faster disease progression and lower survival rate. To achieve this goal, we tested different combinations of radiomics features selectors and machine learning algorithms in an harmonized dataset.

2. Materials and methods

2.1. Participants

We included patients from two different acquisition sites: the Center for Neurodegenerative Diseases and the Aging Brain of the University of Bari Aldo Moro at Pia Fondazione "Card. G. Panico" ('*Scanner 1*', 25 patients with ALS, 24 controls) and the Neurology Unit of Azienda Ospedaliero-Universitaria Consorziale Policlinico Bari ('*Scanner* 2', 48 patients with ALS and 20 healthy controls; '*Scanner 3*', 11 patients with ALS and 10 healthy controls).

ALS-mimicking diseases were excluded after a complete diagnostic work-up including hematological and cerebrospinal fluid analyses, electroneurography, electromyography (de Carvalho et al., 2008) and motor evoked potential (Zoccolella et al., 2020). None of patients met the Strong criteria for ALS-Frontotemporal dementia (Strong et al., 2017). Based on clinical and instrumental examination, patients were classified as "Classical" ALS phenotype (n = 57) and "non-Classical" ALS phenotypes (n = 27, including 9 subjects with Bulbar ALS, 4 with Flail arm/leg and 14 (7/7) with PLMN and PUMN phenotypes).

Demographic and clinical variables were collected during the diagnostic work-up including: age at diagnosis (acquired during first neurological clinical evaluation), age at symptom onset (AAO), onset to diagnosis interval (ODI), site of onset and clinical phenotypes according to the classification system (Chiò et al., 2011). All patients were evaluated with ALS Functional Rating Scale-Revised (ALSFRS-r) (Cedarbaum et al., 1999).

The control group was selected according to ADNI-3 criteria (Weiner et al., 2017) excluding subjects with evidence of autoimmune, inflammatory, vascular or neurodegenerative diseases. None of the controls had a family history of ALS, and brain MRI abnormalities. The study was conducted in accordance with the Declaration of Helsinki and approved by the local health trust's ethics committees. Written informed consent was obtained from all participants.

2.2. MRI acquisition

All subjects underwent T1-weighted MRI at time of first neurological evaluation. For 'Scanner 1', 3D-structural MRI were acquired on a 3 T scanner (Philips Ingenia 3.0 T) using a Fast-Field Echo (FFE) sequence (repetition time = 8.2 ms, echo time = 3.8 ms, flip angle = 8°, resolution = 256 × 256, slices = 200, thickness = 1 mm and field of view = 250 mm). For 'Scanner 2', participants underwent an MRI on a Philips MRI system 1.5 T scanner using a T1-weighted MP-RAGE (Magnetization-Prepared Rapid Acquisition with Gradient Echo) sequence (repetition time = 25 ms, echo time = 4.6 ms, flip angle = 30°, resolution = 256 × 256, slices = 256, thickness = 0.93 mm and field of view = 240 mm). For 'Scanner 3', MRI was performed with a 1.5 Tesla General Electric Signa MR system using a T1-weighted SPGR (Spoiled Gradient Echo) sequence (repetition time = 26 ms, echo time = 7 ms, flip angle = 50°, resolution = 256 × 256, slices = 200, thickness = 1 mm and field of view = 250 mm). Fluid-attenuated inversion recovery (FLAIR) and T2-weighted MRI sequences were performed in both sites to exclude brain abnormalities, including lacunar and extensive cerebrovascular lesions.

2.3. Radiomics feature extraction

A complete description of the processing pipeline is reported in Fig. 1. Pre-processing of T1-MR images was performed through FreeSurfer (version 7.0) image analysis software (https://surfer.nmr.mgh.harvard.edu/). The toolbox included a first step for removal of non-brain tissue and bias from each structural brain image. Then, the non-uniform intensity corrected image (*nu.mgz*) in the Freesurfer space was used to compute radiomics features. The anatomical labels of the Desikan–Killiany atlas (Desikan et al., 2006) were used to extract the Regions-Of-Interests (ROIs) from the individual cortical and subcortical segmentation image (*aparc* + *aseg.mgz*) considering the following areas in the left and right cerebral hemispheres separately: inferior temporal gyrus, middle temporal gyrus, superior temporal gyrus, paracentral lobule, precentral gyrus, thalamus, caudate, putamen, amygdala and hippocampus. Additionally, midbrain, pons, and medulla oblongata ROIs were obtained using "*segmentBS.sh*" script from FreeSurfer. ROIs were selected according to literature findings on imaging impairment in ALS (Grolez et al., 2016). Segmentation was conducted using a Bayesian parcellation approach relying on a probabilistic atlas of brainstem and neighboring anatomical structures (Iglesias et al., 2015). Subsequentially the binary masks of specific ROIs per subject were obtained by a thresholding step using FSL tools (Smith et al., 2004).

For each ROI, we extracted 88 radiomics features, including first and second order textural measures that highlight spatial distribution of voxels through four different matrices: i) Gray Level Cooccurrence

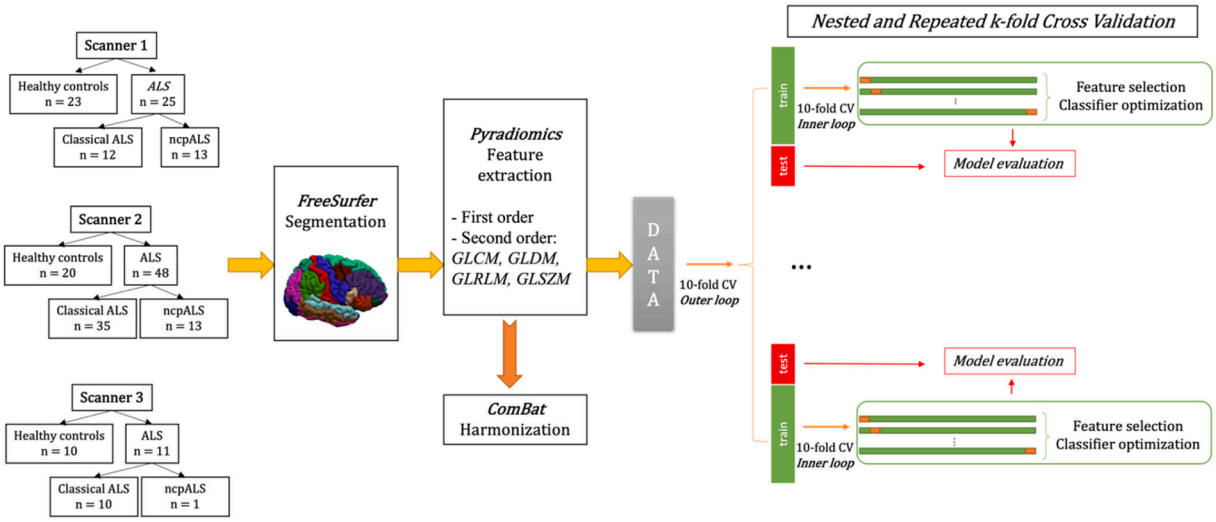

Fig. 1. Processing pipeline. Abbreviations: non-Classical phenotype Amyotrophic Lateral Sclerosis (ncpALS); Gray Level Cooccurrence Matrices (GLCM); Gray Level Run Length Matrices (GLRLM); Gray Level Dependence Matrices (GLDM); Gray Level Size Zone Matrices (GLSZM); Cross Validation (CV).

Matrices (GLCM); ii) Gray Level Run Length Matrices (GLRLM); iii) Gray Level Dependence Matrices (GLDM); and iv) Gray Level Size Zone Matrices (GLSZM) (all extracted features are reported in Supplementary Table 1) (Zwanenburg et al., 2020). The extraction procedure was implemented using Pyradiomics, an open-source Python package (van Griethuysen et al., 2017).

2.4. Radiomics feature harmonization

Combat-based harmonization of radiomics features was carried out to reduce the batch effect resulting from MRI acquisition performed at two sites with different scanners and acquisition protocols. This processing estimates site-specific transformation to express radiomics data in a common space, and has provided satisfactory results also for relatively small datasets (Goh et al., 2017; Johnson et al., 2007; Tafuri, Lombardi, et al., 2022). As implemented for multiple measures on several brain regions, features harmonization was computed using Empirical Bayes framework. Only healthy controls were considered for the estimation of the site hyperparameters of the distributions for site-effect correction. Moreover, to ensure unbiased results, the batch effect was estimated in the training sample of each cross-validation fold and then applied on the remaining subjects in test folds. The R code for implementing the harmonization framework is available in the work by Radua et al.

(Radua et al., 2020).

2.5. Radiomics feature selection

Features selection and classification algorithms were implemented using R software (R Core Team, 2021). In order to reduce dimensionality, avoid collinearity and minimize the potential overfitting due to the huge number of radiomics measures, all radiomics studies consider different features selection methods to define the best predictors for the classification algorithm (Lambin et al., 2017). We considered three feature selection models: 1) Least Absolute Shrinkage and Selection Operator (LASSO); 2) Random Forest Recursive Feature Elimination (RF-RFE) and 3) Maximum Relevance — Minimum Redundancy (mRMR). LASSO defines the optimal penalty parameter minimizing "Binomial Deviance" and features with non-zero regression coefficients are retained (Friedman et al., 2010; Tibshirani, 1996). RF-RFE (Gregorutti et al., 2017) and mRMR (Ding & Peng, 2005) rank features by importance and retain an optimal number proportional to $\sqrt{N}$ (where N is the sample size) according to the method by Hua et al. (Hua et al., 2005). In particular, RF-RFE recursively eliminates features focusing on the performance improvement of the selected measures on the classification task. Conversely, mRMR, considers simultaneously redundancy of features to maximize the dependency between the joint distribution of the selected features and the classification variable.

2.6. Classification analyses

Four machine learning algorithms were combined using the previously selected radiomics features, namely: i) Support Vector Machine (SVM); ii) XGBoost; iii) Random Forest (RF) and iv) K-nearest neighbors (kNN). The choice of classical machine learning methods rather than deep learning framework was carried out due to the relatively small sample size. Deep learning requires thousands of images to work well and for small dataset is more prone to overfitting.

For SVM classifier we used the libSVM package (Chang & Lin, 2011) and adopted a grid search method using a 10-fold cross-validation (CV) approach on the training sets to optimize the hyperparameters of SVM (a *GridSearch* was conducted for (c, C), varying along a grid with c = 0.1, 0.5, 1, 2, 3, 4, and C = 0.001, 0.01, 0.1, 1, 5, 10, where c is the width of the RBF, and C controls the trade-off between having zero training errors and allowing misclassification). Concerning XGBoost's hyperparameters (https://xgboost.ai), we implemented a tuning for the tree-based learners (number of trees from 100 to 500, max_depth from 1 to 10, shrinkage from 0.1 to 0.5 and L2 regularization from −1 to 0) in a 10-fold CV setting. The "objective" hyperparameter, that defines the loss function to be used, was set to "binary:logistic" as for classification problems with probability estimation (Gonçalves et al., 2022). For the RF classifier we tuned the number (n = 1000, 1500, 2000, 2500) and maximum (n = 1:5) depth of the tree.

In our framework, we considered binary comparisons between healthy controls and ALS patients and between the group of "Classical" and "non-Classical" ALS subjects. Of note, the Majority Weighted Minority Oversampling Technique (MWMOTE) was used to handle possible imbalanced learning problems for each initial dataset, allowing to generate additional samples for minority classes (Barua et al., 2014).

2.7. Statistical analysis

Data for each group were explored using descriptive statistics (mean ± standard deviation). Group differences in age, gender, ODI, type of onset, clinical phenotypes and ALSFRS-r values were investigated through Chi-square test, one-way analysis of variance (ANOVA) and

Kruskal–Wallis ANOVA. To assess survival, we performed a Two-Steps cluster analysis including reaching or not the event death or tracheostomy (as categorical variable) and time to the last follow-up (as continuous variable) and thus dichotomized ALS patients into long and short survivors (Benassi et al., 2020; Chiu et al., 2001; Milella et al., 2022). For all analyses, the corrected significance threshold was set at $p < 0.05$.

As regards classification analyses, each combination of the three feature selection models and four classification algorithms was evaluated in a ten times repeated 10-fold CV (Lampe et al., 2022; Zhu et al., 2018). The feature selection methods were included in the inner loop of each outer loop of CV. Selected features were used to optimize and train each classification algorithm and the best model was used to test the predictive performances of the model.

Accuracy, sensitivity, specificity and the area under the receiver operating characteristic curve (AUC), mediated over the 100 bootstraps of classification, were calculated for each model. The different classification algorithms were compared through Friedman test followed by pairwise comparison using the Wilcoxon signed-rank test in cases of statistically significant differences. Bonferroni method was used to account for multiple comparisons and an adjusted alpha (α) level of < 0.05 was considered statistically significant (Wong, 2017).

A frequency-based criterion was used to select the most stable radiomics features according to the different feature selectors. At each round of the bootstrap, the features selected by LASSO, RF-RFE and mRMR respectively were stored and the radiomics features that occurred in at least 95° percentile of the frequency vector were considered the most stable. Statistical analysis was performed using R software (Version 3.6.3: R Core Team, 2021).

3. Results

3.1. Demographic and clinical characteristics

Demographic and clinical data for healthy controls (HC) and ALS cases are reported in Table 1. For statistical purpose, also given the expected higher prevalence of "Classical" ALS compared to those with "non-Classical" form of the disease, these latter patients were considered at once and were defined as "non-Classical" ALS. No statistical differences emerged in age and sex distributions between HC and ALS patients. Demographic and clinical data for "Classical" ALS phenotype and "non-Classical" ALS phenotypes are reported in Table 2. "Classical" ALS patients showed a shorter interval between onset and death and were more likely to have short survival time compared to "non-Classical" ALS phenotypes patients. No further statistically significant differences were observed.

Table 1
Demographic and clinical information of healthy controls (HC) and Amyotrophic Lateral Sclerosis (ALS) patients.

	ALS (n = 84)	HC (n = 53)	p-value
	Mean ± SD or %	Mean ± SD or %	
Scanner/Protocol (%)			0.086
Scanner 1	25 (29.8)	23 (43.4)	
Scanner 2	48 (57.1)	20 (37.7)	
Scanner 3	11 (13.1)	10 (18.9)	
Male Gender (%)	45 (53.6)	27 (50.9)	0.901
Age at Sampling, years	60.67 (11.13)	61.85 (8.39)	0.508
Age at symptoms onset, years	59.67 (11.28)		
ODI, months	14.47 (12.31)		
ALSFRSr	37.24 (7.52)		
Phenotype ALS (%)			
Bulbar	9 (10.7)		
Classical ALS	57 (67.9)		
Flail arm/leg	4 (4.8)		
PLMN	7 (8.3)		
PUMN	7 (8.3)		
Type of onset (%) [83]			
Bulbar	23 (27.4)		
Spinal	60 (71.4)		

Abbreviations: Standard Deviation (SD); Onset to diagnosis interval (ODI); prevalent lower motor neuron phenotype (PLMN); prevalent upper motor neuron phenotype (PUMN); ALS Functional Rating Scale-Revised (ALSFRS-r).

3.2. ALS classification

Classification performances of radiomics models are reported in Table 3. SVM trained with features selected by LASSO (LASSO-SVM) showed the highest accuracy (0.811 ± 0.114), largest AUC (0.870 ± 0.113) and the best balance between specificity (0.767 ± 0.169) and sensitivity (0.854 ± 0.123).

The Friedman test, conducted to assess differences between the distributions of AUC for all trained models, showed an overall p-value < 0.0001. Post-hoc test (Wilcoxon signed-rank) showed no statistical differences between LASSO-SVM and mRMR-RF, with p-value of 1, and mRMR-SVM model, with p-value of 0.644 (Fig. 2**a**).

The most stable features for each selector are reported in Table 5. The skewness of the gray-level distribution at level of right amygdala resulted the best discriminant feature according to LASSO and mRMR. Moreover, LASSO identified the Size Zone Non Uniformity Normalized from GLSZM matrix of the left thalamus as the best discriminant feature and RFE identified the Gray Level Non Uniformity of the GLDM matrix of the left precentral gyrus.

3.3. Classical ALS phenotypes classification

The classification performance of radiomics models in discriminating "Classical" ALS from "non-Classical" ALS phenotypes is reported in Table 4, together with values of accuracy, sensitivity, specificity and AUC. The mRMR with SVM classifier resulted the best model showing higher values of accuracy (0.929 ± 0.07), AUC (0.985 ± 0.031), specificity (0.962 ± 0.113), sensitivity (0.895 ± 0.112). Friedman test showed significant differences between models with a p-value < 0.0001. Post-hoc pairwise comparisons revealed that it outperformed all other models (Fig. 2**b**).

As most stable radiomics features, we found two measures with mRMR (Table 5). The best features belonged to the right subcortical regions namely hippocampus, thalamus, besides the paracentral lobule and pons from the brainstem.

4. Discussion

In this study we explored, for the first time, the usefulness of radiomics analysis on T1-weighted MR images in distinguish ALS

Table 2
Demographic and clinical information of "Classical" and "non-Classical" phenotypes of ALS patients.

	"Classical" ALS (n = 57)	"non-Classical" ALS (n = 27)	p-value
	Mean ± SD or %	Mean ± SD or %	
Male Gender (%)	31 (54.4)	14 (51.9)	1.000
Age at Sampling, years	61.49 (11.20)	58.93 (10.99)	0.327
Age at symptoms onset, years	60.65 (11.23)	57.61 (11.29)	0.250
ODI, months	12.60 (9.19)	18.42 (16.69)	0.043
ALSFRSr	36.47 (7.75)	39.47 (6.49)	0.135
Short Survival (%)	44 (77.2)	14 (51.9)	0.036
Type of onset (%) [83]			
Bulbar	14 (24.6)	9 (33.3)	
Spinal	43 (75.4)	17 (63.0)	

Abbreviations: Standard Deviation (SD); Onset to diagnosis interval (ODI); pure lower motor neuron phenotype (PLMN); pure upper motor neuron phenotype (PUMN); ALS Functional Rating Scale-Revised (ALSFRS-r).

Table 3
Performance metrics (mean and standard deviation) for HC vs ALS models, averaged over 100 bootstraps.

Features selector	*Classifier*	*Accuracy*	*AUC*	*Sensitivity*	*Specificity*
LASSO	**SVM**	**0.811 (0.114)**	**0.870 (0.113)**	**0.854 (0.123)**	**0.767 (0.169)**
RFE	SVM	0.705 (0.121)	0.764 (0.127)	0.727 (0.18)	0.684 (0.214)
mRMR	**SVM**	**0.739 (0.13)**	**0.824 (0.121)**	**0.738 (0.19)**	**0.739 (0.193)**
LASSO	kNN	0.664 (0.124)	0.689 (0.12)	0.523 (0.155)	0.804 (0.203)
RFE	kNN	0.638 (0.096)	0.707 (0.127)	0.57 (0.196)	0.706 (0.164)
mRMR	kNN	0.596 (0.116)	0.663 (0.141)	0.525 (0.174)	0.667 (0.183)
LASSO	RF	0.748 (0.109)	0.828 (0.114)	0.703 (0.125)	0.794 (0.156)
RFE	RF	0.679 (0.141)	0.735 (0.14)	0.634 (0.183)	0.723 (0.2)
mRMR	RF	0.721 (0.111)	0.821 (0.133)	0.705 (0.178)	0.737 (0.224)
LASSO	XGBoost	0.744 (0.111)	0.808 (0.13)	0.717 (0.125)	0.771 (0.166)
RFE	XGBoost	0.645 (0.132)	0.692 (0.148)	0.609 (0.171)	0.681 (0.183)
mRMR	XGBoost	0.706 (0.125)	0.778 (0.139)	0.691 (0.188)	0.72 (0.194)

Abbreviations: Least Absolute Shrinkage and Selection Operator (LASSO); Random Forest Recursive Feature Elimination (RF-RFE); Maximum Relevance — Minimum Redundancy (mRMR); Random Forest (RF); Support Vector Machine (SVM); K-nearest neighbors (kNN).

patients from healthy controls and patients with "Classical" ALS versus "non-Classical" ALS phenotypes. Radiomics analysis showed good accuracy (81.1 %) in classifying ALS patients respect to controls. Conversely radiomics features were able to distinguish "Classical" ALS from "non-Classical" ALS motor phenotypes with 92.9 % accuracy. Concerning features selection and classification models, support vector machine performed better with radiomics features than to XGBoost, kNN and RF algorithms. Remarkably, the LASSO feature selector demonstrated superior performance when compared to the combination of RF-RFE and mRMR for each type of machine learning algorithm.

Diagnosis of ALS can be exploited with different biomarkers and biomedical signal approaches in combination with machine learning algorithms. Indeed, a recent review (Fernandes et al., 2021) reports that electromiography (EMG), gait rhythm (GT) and MRI are the most widespread signals in this task, also highlighting that if EMG and GT are well established biomarkers with performances of discrimination above

Table 4
Performance metrics (mean and standard deviation) for "Classical" vs "non-Classical" ALS models, averaged over 100 bootstraps.

Features Selector	***Classifier***	***Accuracy***	***AUC***	***Sensitivity***	***Specificity***
LASSO	SVM	0.92 (0.072)	0.957 (0.06)	0.898 (0.1)	0.941 (0.133)
RFE	SVM	0.861 (0.109)	0.935 (0.069)	0.863 (0.159)	0.859 (0.184)
mRMR	**SVM**	**0.929 (0.07)**	**0.985 (0.031)**	**0.895 (0.122)**	**0.962 (0.113)**
LASSO	kNN	0.525 (0.101)	0.514 (0.141)	0.853 (0.16)	0.804 (0.234)
RFE	kNN	0.577 (0.121)	0.613 (0.171)	0.902 (0.126)	0.748 (0.188)
mRMR	kNN	0.523 (0.099)	0.55 (0.153)	0.775 (0.164)	0.729 (0.191)
LASSO	RF	0.807 (0.094)	0.942 (0.071)	0.929 (0.096)	0.686 (0.193)
RFE	RF	0.78 (0.135)	0.873 (0.095)	0.87 (0.139)	0.69 (0.177)
mRMR	RF	0.802 (0.061)	0.881 (0.066)	0.886 (0.124)	0.717 (0.133)
LASSO	XGBoost	0.749 (0.091)	0.895 (0.089)	0.94 (0.087)	0.558 (0.177)
RFE	XGBoost	0.759 (0.131)	0.837 (0.124)	0.89 (0.1)	0.628 (0.211)
mRMR	XGBoost	0.713 (0.129)	0.805 (0.109)	0.817 (0.148)	0.609 (0.203)

Abbreviations: Least Absolute Shrinkage and Selection Operator (LASSO); Random Forest Recursive Feature Elimination (RF-RFE); Maximum Relevance — Minimum Redundancy (mRMR); Random Forest (RF); Support Vector Machine (SVM); K-nearest neighbors (kNN).

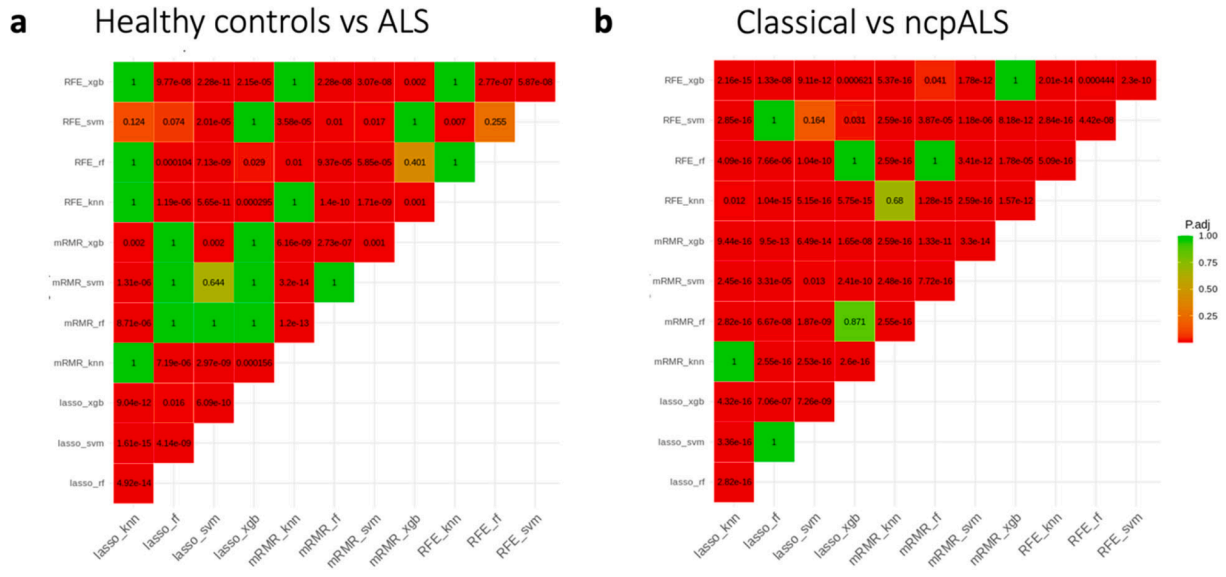

Fig. 2. Pairwise comparison between combined models. Heat maps reports Bonferroni-adjusted p-values for pairwise comparisons of features selection + classification algorithms using the Wilcoxon signed-rank test; Panel (**a**) shows results for model to discriminate ALS from controls and (**b**) for "Classical" ALS from "non-Classical" ALS phenotypes. Abbreviations: non-Classical phenotype Amyotrophic Lateral Sclerosis (ncpALS); Least Absolute Shrinkage and Selection Operator (LASSO); Random Forest Recursive Feature Elimination (RF-RFE); Maximum Relevance — Minimum Redundancy (mRMR); Random Forest (RF); Support Vector Machine (SVM); K-nearest neighbors (kNN).

Table 5
Most stable radiomics features for different feature selection methods as over the 95th percentile of the frequency vector.

Model	*Selector*	*Feature*	*ROI*	*HC*	*ALS*	*p-value*
HC vs ALS	LASSO/mRMR	Skewness	Right Amygdala	−0.05 (0.28)	−0.28 (0.39)	<0.001
HC vs ALS	LASSO	Glszm Size Zone Non Uniformity Normalized	Left Thalamus	−0.36 (0.03)	0.35 (0.03)	0.008
HC vs ALS	RF-RFE	Gldm Gray Level Non Uniformity	Left Precentral	2547.78 (368.84)	2293.36 (536.15)	0.003
Model	*Selector*	*Feature*	*ROI*	*"Classical" ALS*	*"non-Classical" ALS*	*p-value*
ALS variants	mRMR	gldm SmallDependenceLowGrayLevelEmphasis	Right Hippocampus	0.003 (0.001)	0.002 (0.000)	0.003
ALS variant	mRMR	gldm SmallDependenceLowGrayLevelEmphasis	Pons	0.004 (0.002)	0.003 (0.001)	0.04
ALS variant	LASSO	Glcm Correlation	Right Thalamus	0.64 (0.05)	0.68 (0.05)	0.001
ALS variant	RF-RFE	Kurtosis	Right Paracentral	2.48 (0.23)	2.37 (0.13)	0.021

Abbreviations: Least Absolute Shrinkage and Selection Operator (LASSO); Random Forest Recursive Feature Elimination (RF-RFE); Maximum Relevance — Minimum Redundancy (mRMR); Gray Level Size Zone Matrices (GLSZM); Gray Level Dependence Matrices (GLDM).

95 %, the discovery of a MRI biomarker with comparable classification capabilities remains an open challenge. In recent years, several studies have investigated the usefulness of imaging biomarkers, alone or in combination with clinical data and multimodal MRI, for diagnostic and prognostic purpose in ALS. Ferraro et al. reported that the cortical thickness at the level of precentral gyrus showed an accuracy of 86 % in distinguishing ALS patients from controls, albeit considering a single-cohort of patients for model training (Ferraro et al., 2017). Similarly, Thome et al. focused on the classification of ALS from controls using both structural and functional MRI data. The RF classifier trained on volumetric features achieved an accuracy of 59.66 %, with specificity of 66.93 %, and sensitivity of 52.38 % (Thome et al., 2022). More recently, Rajagopalan et al. assessed whether MRI metrics were able to identify four different phenotypes of ALS patients, namely PUMN with or without corticospinal tract hyperintensity, "Classical" ALS and ALS-FTD. The authors showed that Random Forest algorithm displays the best performance in classifying the ALS phenotypes with an accuracy ranging from 70 to 94 % for the different combination of imaging biomarkers. In the latter study white matter metrics showed far superior performance in classifying ALS phenotypes compared to clinical measures or gray matter metrics (Rajagopalan et al., 2023).

Overall, our results on radiomic analysis were comparable with the state-of-art discrimination models, confirming the difficulty in discriminating ALS from controls using structural imaging measures, also considering second order statistical morphometric measures. This evidence reflects the extreme phenotypic variability of the ALS disease which did not allows clinicians to identify a single discriminant neuroanatomical region. Noteworthy, as previous MRI studies conducted on gray matter, the most significant brain regions for distinguishing ALS patients from healthy controls were found in limbic areas (i.e., the right amygdala, right hippocampus, and left superior temporal lobe). Although the involvement of these regions in ALS has been reported in previous pathology and neuroimaging studies (Bede et al., 2017; Machts et al., 2018; Pinkhardt et al., 2006), their discriminant role has not been extensively examined. Importantly, the skewness of the right amygdala, selected through both LASSO and mRMR, highlighted a significant asymmetric distribution of the gray levels for this region for ALS patients, confirming a distinctive pattern of amygdala atrophy probably associated with the more advanced stages of the disease (Liu et al., 2022).

Concerning the classification performance of models "Classical" versus "non-Classical" ALS phenotypes, no previous studies have implemented a discrimination model. Among all the neuroanatomical structures examined, the hippocampus emerged as one of the most discriminative. The extensive literature on the radiological involvement of hippocampal circuits in ALS disease supports this finding (Anderson et al., 1995; Grosskreutz et al., 2006; Kato et al., 1997). A recent review highlighted episodic memory dysfunction in ALS occurs in addition to the typical executive dysfunctions associated with the ALS-frontotemporal dementia spectrum (Christidi et al., 2018).

Additionally, the pons of brainstem and paracentral area were found to be the most discriminative and stable neuroanatomical regions in differentiating "Classical" versus "non-Classical" ALS phenotypes. These results are consistent with the well-established pathological model of ALS, which identifies these structures as involved in the early stage of the disease (Brettschneider et al., 2013). Therefore, it could be speculated that in "Classical" ALS patients, the brainstem and motor areas are involved early on, whereas in "non-Classical" ALS phenotypes the pathological process could start in different neuroanatomical regions. Similar results were reported by previous data-driven analyses that showed the relative preservation of the brainstem structures only in a small subgroup of ALS patients (Milella et al., 2023; Tan et al., 2022). We extended these results by showing that the patients with none or less involvement of the brainstem structures belonged to the "non-Classical" group of ALS patients. Not surprisingly, in our cohort these latter patients were characterized by longer survival, confirming the role of the brainstem structures in the survival in ALS disease, as reported elsewhere (Milella et al., 2022).

This study had several limitations. First, the most important limitation was the absence of an external and independent validation cohort which limits the generalization of results. However, although our models did not use an independent dataset to test the performances, we statistically accounted for this issue using a nested cross-validation training with bootstrapping. Secondly, acknowledging the constraint of grouping significantly different ALS phenotypes as a single group is both clinically and biologically inappropriate, the small number of subjects per phenotypes did not allows a sufficient statistical power to define a multiclass classifier or a cascade diagnostic model. Further investigations, also improving the sample size for each specific phenotypes, could enable to design a suitable differential diagnosis support system. Finally, new studies with multicentric and larger sample size, also with combined set of clinical/radiological data are needed to confirm our results.

5. Conclusions

Application of radiomics potentiality on ALS discrimination can help the comprehension of the disruptive process of the brain affected by this fatal disease, also capturing invisible markers over images. Indeed, our radiomics approach was able to extrapolate new discriminative radiological features without any other complementary demographic, clinical or genetic information, also comparable with volumetric features. Furthermore, the excellent performance of "Classical" ALS phenotype classification models could define a new simpler stratification approach based only on radiological acquisition, could help to improve diagnosis and may prove useful to assess disease severity and longitudinally monitor ALS patients along the disease course. Finally, our finding aligns with aims of the Sustainable Development Goals of the United Nations

2030 Agenda (Take Action for the Sustainable Development Goals - United Nations Sustainable Development; Transforming Our World: The 2030 Transforming our world: The 2030 Agenda for Sustainable Development | Department of Economic and Social Affairs), which emphasize the need to identify imaging features that could serve as reliable and accessible biomarkers for ALS across countries and ages.

CRediT authorship contribution statement

Benedetta Tafuri: Conceptualization, Formal analysis, Methodology, Software, Visualization, Writing – original draft. **Giammarco Milella:** Conceptualization, Methodology, Validation, Supervision, Writing – review & editing. **Marco Filardi:** Methodology, Supervision, Validation, Writing – review & editing. **Alessia Giugno:** Data curation, Resources, Writing – review & editing. **Stefano Zoccolella:** Data curation, Resources, Writing – review & editing. **Ludovica Tamburrino:** Data curation, Resources, Writing – review & editing. **Valentina Gnoni:** Data curation, Resources, Writing – review & editing. **Daniele Urso:** Data curation, Resources, Writing – review & editing. **Roberto De Blasi:** Validation, Visualization, Writing – review & editing. **Salvatore Nigro:** Conceptualization, Project administration, Supervision, Writing – review & editing. **Giancarlo Logroscino:** Funding acquisition, Conceptualization, Project administration, Supervision, Writing – review & editing.

Declaration of Competing Interest

The authors declare the following financial interests/personal relationships which may be considered as potential competing interests: Giancarlo Logroscino reports financial support was provided by Puglia Region. Giancarlo Logroscino reports a relationship with Roche that includes: consulting or advisory.

Data availability

Data will be made available on request.

Acknowledgements

This work was supported by Regione Puglia (DGR No. 1284 - 27.05.2015) for the project Registro Regionale per la SLA, la FTD-P e le patologie affini in Regione Puglia (SLAPDem registerhttps://www.slapdem.it). This work has been also supported with the funding of Regione Puglia and CNR for Tecnopolo per la Medicina di Precisione. D. G.R. No. 2117 of 21.11.2018 (CUPB84I18000540002) — C.I.R.E.M.I.C (Research Center of Excellence for Neurodegenerative Diseases and Brain Aging)—University of Bari "Aldo Moro."

Code availability

The underlying code for this study [and training/validation datasets] is not publicly available but may be made available to qualified researchers on reasonable request from the corresponding author.

Appendix A. Supplementary data

Supplementary data to this article can be found online at https://doi.org/10.1016/j.eswa.2023.122585.

References

Anderson, V. E., Cairns, N. J., & Leigh, P. N. (1995). Involvement of the amygdala, dentate and hippocampus in motor neuron disease. *Journal of the Neurological Sciences, 129*(Suppl), 75–78. https://doi.org/10.1016/0022-510x(95)00069-e

Barua, S., Islam, M. M., Yao, X., & Murase, K. (2014). MWMOTE–Majority Weighted Minority Oversampling Technique for Imbalanced Data Set Learning. *IEEE Transactions on Knowledge and Data Engineering, 26*(2), 405–425. https://doi.org/10.1109/TKDE.2012.232

Bede, P., Bokde, A., Elamin, M., Byrne, S., McLaughlin, R. L., Jordan, N., Hampel, H., Gallagher, L., Lynch, C., Fagan, A. J., Pender, N., & Hardiman, O. (2013). Grey matter correlates of clinical variables in amyotrophic lateral sclerosis (ALS): A neuroimaging study of ALS motor phenotype heterogeneity and cortical focality. *Journal of Neurology, Neurosurgery, and Psychiatry, 84*(7), 766–773. https://doi.org/10.1136/jnnp-2012-302674

Bede, P., Iyer, P. M., Finegan, E., Omer, T., & Hardiman, O. (2017). Virtual brain biopsies in amyotrophic lateral sclerosis: Diagnostic classification based on in vivo pathological patterns. *NeuroImage : Clinical, 15*, 653–658. https://doi.org/10.1016/j.nicl.2017.06.010

Benassi, M., Garofalo, S., Ambrosini, F., Sant'Angelo, R. P., Raggini, R., De Paoli, G., Ravani, C., Giovagnoli, S., Orsoni, M., & Piraccini, G. (2020). Using Two-Step Cluster Analysis and Latent Class Cluster Analysis to Classify the Cognitive Heterogeneity of Cross-Diagnostic Psychiatric Inpatients. *Frontiers in Psychology, 11*, 1085. https://doi.org/10.3389/fpsyg.2020.01085

Brettschneider, J., Del Tredici, K., Toledo, J. B., Robinson, J. L., Irwin, D. J., Grossman, M., Suh, E., Van Deerlin, V. M., Wood, E. M., Baek, Y., Kwong, L., Lee, E. B., Elman, L., McCluskey, L., Fang, L., Feldengut, S., Ludolph, A. C., Lee, V.-M.-Y., Braak, H., & Trojanowski, J. Q. (2013). Stages of pTDP-43 pathology in amyotrophic lateral sclerosis. *Annals of Neurology, 74*(1), 20–38. https://doi.org/10.1002/ana.23937

Brooks, B. R. (1994). El Escorial World Federation of Neurology criteria for the diagnosis of amyotrophic lateral sclerosis. Subcommittee on Motor Neuron Diseases/Amyotrophic Lateral Sclerosis of the World Federation of Neurology Research Group on Neuromuscular Diseases and the El Escorial "Clinical limits of amyotrophic lateral sclerosis" workshop contributors. *Journal of the Neurological Sciences, 124*(Suppl), 96–107. https://doi.org/10.1016/0022-510x(94)90191-0

Brooks, B. R., Miller, R. G., Swash, M., Munsat, T. L., & World Federation of Neurology Research Group on Motor Neuron Diseases. (2000). El Escorial revisited: Revised criteria for the diagnosis of amyotrophic lateral sclerosis. *Amyotrophic Lateral Sclerosis and Other Motor Neuron Disorders: Official Publication of the World Federation of Neurology, Research Group on Motor Neuron Diseases, 1*(5), 293–299. https://doi.org/10.1080/146608200300079536

Cedarbaum, J. M., Stambler, N., Malta, E., Fuller, C., Hilt, D., Thurmond, B., & Nakanishi, A. (1999). The ALSFRS-R: A revised ALS functional rating scale that incorporates assessments of respiratory function. BDNF ALS Study Group (Phase III). *Journal of the Neurological Sciences, 169*(1–2), 13–21. https://doi.org/10.1016/s0022-510x(99)00210-5

Chang, C., & Lin, C. (2011). LIBSVM: A library for support vector machines. *ACM Transactions on Intelligent Systems and Technology*.

Cheung, E. Y. W., Chau, A. C. M., Tang, F. H., & On Behalf Of The Alzheimer's Disease Neuroimaging Initiative, null. (2022). Radiomics-Based Artificial Intelligence Differentiation of Neurodegenerative Diseases with Reference to the Volumetry. *Life (Basel, Switzerland), 12*(4), 514. https://doi.org/10.3390/life12040514

Chiò, A., Calvo, A., Moglia, C., Mazzini, L., Mora, G., & PARALS Study Group. (2011). Phenotypic heterogeneity of amyotrophic lateral sclerosis: A population based study. *Journal of Neurology, Neurosurgery, and Psychiatry, 82*(7), 740–746. https://doi.org/10.1136/jnnp.2010.235952

Chiu, T., Fang, D., Chen, J., Wang, Y., & Jeris, C. (2001). A robust and scalable clustering algorithm for mixed type attributes in large database environment. In *Proceedings of the Seventh ACM SIGKDD International Conference on Knowledge Discovery and Data Mining* (pp. 263–268). https://doi.org/10.1145/502512.502549

Christidi, F., Karavasilis, E., Velonakis, G., Ferentinos, P., Rentzos, M., Kelekis, N., Evdokimidis, I., & Bede, P. (2018). The Clinical and Radiological Spectrum of Hippocampal Pathology in Amyotrophic Lateral Sclerosis. *Frontiers in Neurology, 9*, 523. https://doi.org/10.3389/fneur.2018.00523

Ciccarelli, O., Behrens, T. E., Johansen-Berg, H., Talbot, K., Orrell, R. W., Howard, R. S., Nunes, R. G., Miller, D. H., Matthews, P. M., Thompson, A. J., & Smith, S. M. (2009). Investigation of white matter pathology in ALS and PLS using tract-based spatial statistics. *Human Brain Mapping, 30*(2), 615–624. https://doi.org/10.1002/hbm.20527

de Carvalho, M., Dengler, R., Eisen, A., England, J. D., Kaji, R., Kimura, J., Mills, K., Mitsumoto, H., Nodera, H., Shefner, J., & Swash, M. (2008). Electrodiagnostic criteria for diagnosis of ALS. *Clinical Neurophysiology: Official Journal of the International Federation of Clinical Neurophysiology, 119*(3), 497–503. https://doi.org/10.1016/j.clinph.2007.09.143

Desikan, R. S., Ségonne, F., Fischl, B., Quinn, B. T., Dickerson, B. C., Blacker, D., Buckner, R. L., Dale, A. M., Maguire, R. P., Hyman, B. T., Albert, M. S., & Killiany, R. J. (2006). An automated labeling system for subdividing the human cerebral cortex on MRI scans into gyral based regions of interest. *NeuroImage, 31*(3), 968–980. https://doi.org/10.1016/j.neuroimage.2006.01.021

Ding, C., & Peng, H. (2005). Minimum redundancy feature selection from microarray gene expression data. *Journal of Bioinformatics and Computational Biology, 3*(2), 185–205. https://doi.org/10.1142/s0219720005001004

Fernandes, F., Barbalho, I., Barros, D., Valentim, R., Teixeira, C., Henriques, J., Gil, P., & Júnior, M. D. (2021). Biomedical signals and machine learning in amyotrophic lateral sclerosis: A systematic review. *BioMedical Engineering OnLine, 20*. https://doi.org/10.1186/s12938-021-00896-2

Ferraro, P. M., Agosta, F., Riva, N., Copetti, M., Spinelli, E. G., Falzone, Y., Sorarù, G., Comi, G., Chiò, A., & Filippi, M. (2017). Multimodal structural MRI in the diagnosis of motor neuron diseases. *NeuroImage. Clinical, 16*, 240–247. https://doi.org/10.1016/j.nicl.2017.08.002

Fratello, M., Caiazzo, G., Trojsi, F., Russo, A., Tedeschi, G., Tagliaferri, R., & Esposito, F. (2017). Multi-View Ensemble Classification of Brain Connectivity Images for

Neurodegeneration Type Discrimination. *Neuroinformatics, 15*(2), 199–213. https://doi.org/10.1007/s12021-017-9324-2

Friedman, J., Hastie, T., & Tibshirani, R. (2010). Regularization Paths for Generalized Linear Models via Coordinate Descent. *Journal of Statistical Software, 33*(1), 1–22.

Goh, W. W. B., Wang, W., & Wong, L. (2017). Why Batch Effects Matter in Omics Data, and How to Avoid Them. *Trends in Biotechnology, 35*(6), 498–507. https://doi.org/10.1016/j.tibtech.2017.02.012

Gonçalves, M., Gsaxner, C., Ferreira, A., Li, J., Puladi, B., Kleesiek, J., Egger, J., & Alves, V. (2022). Radiomics in Head and Neck Cancer Outcome Predictions. *Diagnostics, 12*(11), 2733. https://doi.org/10.3390/diagnostics12112733

Gregorutti, B., Michel, B., & Saint-Pierre, P. (2017). Correlation and variable importance in random forests. *Statistics and Computing, 27*(3), 659–678. https://doi.org/10.1007/s11222-016-9646-1

Grolez, G., Moreau, C., Danel-Brunaud, V., Delmaire, C., Lopes, R., Pradat, P. F., El Mendili, M. M., Defebvre, L., & Devos, D. (2016). The value of magnetic resonance imaging as a biomarker for amyotrophic lateral sclerosis: A systematic review. *BMC Neurology, 16*(1), 155. https://doi.org/10.1186/s12883-016-0672-6

Grollemund, V., Pradat, P.-F., Querin, G., Delbot, F., Le Chat, G., Pradat-Peyre, J.-F., & Bede, P. (2019). Machine Learning in Amyotrophic Lateral Sclerosis: Achievements, Pitfalls, and Future Directions. *Frontiers in Neuroscience, 13*, 135. https://doi.org/10.3389/fnins.2019.00135

Grosskreutz, J., Kaufmann, J., Frädrich, J., Dengler, R., Heinze, H.-J., & Peschel, T. (2006). Widespread sensorimotor and frontal cortical atrophy in Amyotrophic Lateral Sclerosis. *BMC Neurology, 6*, 17. https://doi.org/10.1186/1471-2377-6-17

Hannaford, A., Pavey, N., van den Bos, M., Geevasinga, N., Menon, P., Shefner, J. M., Kiernan, M. C., & Vucic, S. (2021). Diagnostic Utility of Gold Coast Criteria in Amyotrophic Lateral Sclerosis. *Annals of Neurology, 89*(5), 979–986. https://doi.org/10.1002/ana.26045

Hardiman, O., van den Berg, L. H., & Kiernan, M. C. (2011). Clinical diagnosis and management of amyotrophic lateral sclerosis. *Nature Reviews. Neurology, 7*(11), 639–649. https://doi.org/10.1038/nrneurol.2011.153

Hua, J., Xiong, Z., Lowey, J., Suh, E., & Dougherty, E. R. (2005). Optimal number of features as a function of sample size for various classification rules. *Bioinformatics (Oxford, England), 21*(8), 1509–1515. https://doi.org/10.1093/bioinformatics/bti171

Iglesias, J. E., Van Leemput, K., Bhatt, P., Casillas, C., Dutt, S., Schuff, N., Truran-Sacrey, D., Boxer, A., Fischl, B., & Alzheimer's Disease Neuroimaging Initiative. (2015). Bayesian segmentation of brainstem structures in MRI. *NeuroImage, 113*, 184–195. https://doi.org/10.1016/j.neuroimage.2015.02.065

Jain, M., Rai, C. S., & Jain, J. (2021). A Novel Method for Differential Prognosis of Brain Degenerative Diseases Using Radiomics-Based Textural Analysis and Ensemble Learning Classifiers. *Computational and Mathematical Methods in Medicine, 2021*, 7965677. https://doi.org/10.1155/2021/7965677

Johnson, W. E., Li, C., & Rabinovic, A. (2007). Adjusting batch effects in microarray expression data using empirical Bayes methods. *Biostatistics (Oxford, England), 8*(1), 118–127. https://doi.org/10.1093/biostatistics/kxj037

Kato, Y., Matsumura, K., Kinosada, Y., Narita, Y., Kuzuhara, S., & Nakagawa, T. (1997). Detection of pyramidal tract lesions in amyotrophic lateral sclerosis with magnetization-transfer measurements. *AJNR. American Journal of Neuroradiology, 18*(8), 1541–1547.

Kiernan, M. C., Vucic, S., Cheah, B. C., Turner, M. R., Eisen, A., Hardiman, O., Burrell, J. R., & Zoing, M. C. (2011). Amyotrophic lateral sclerosis. *Lancet (London, England), 377*(9769), 942–955. https://doi.org/10.1016/S0140-6736(10)61156-7

Lambin, P., Leijenaar, R. T. H., Deist, T. M., Peerlings, J., de Jong, E. E. C., van Timmeren, J., Sanduleanu, S., Larue, R. T. H. M., Even, A. J. G., Jochems, A., van Wijk, Y., Woodruff, H., van Soest, J., Lustberg, T., Roelofs, E., van Elmpt, W., Dekker, A., Mottaghy, F. M., Wildberger, J. E., & Walsh, S. (2017). Radiomics: The bridge between medical imaging and personalized medicine. *Nature Reviews. Clinical Oncology, 14*(12), 749–762. https://doi.org/10.1038/nrclinonc.2017.141

Lampe, L., Niehaus, S., Huppertz, H.-J., Merola, A., Reinelt, J., Mueller, K., … Schroeter, M. L. (2022). Comparative analysis of machine learning algorithms for multi-syndrome classification of neurodegenerative syndromes. *Alzheimer's Research & Therapy, 14*(1), 62. https://doi.org/10.1186/s13195-022-00983-z

Liu, S., Zhao, Y., Ren, Q., Zhang, D., Shao, K., Lin, P., Yuan, Y., Dai, T., Zhang, Y., Li, L., Li, W., Shan, P., Meng, X., Wang, Q., & Yan, C. (2022). Amygdala abnormalities across disease stages in patients with sporadic amyotrophic lateral sclerosis. *Human Brain Mapping, 43*(18), 5421–5431. https://doi.org/10.1002/hbm.26016

Logroscino, G., & Piccininni, M. (2019). Amyotrophic Lateral Sclerosis Descriptive Epidemiology: The Origin of Geographic Difference. *Neuroepidemiology, 52*(1–2), 93–103. https://doi.org/10.1159/000493386

Machts, J., Vielhaber, S., Kollewe, K., Petri, S., Kaufmann, J., & Schoenfeld, M. A. (2018). Global Hippocampal Volume Reductions and Local CA1 Shape Deformations in Amyotrophic Lateral Sclerosis. *Frontiers in Neurology, 9*, 565. https://doi.org/10.3389/fneur.2018.00565

Milella, G., Introna, A., Ghirelli, A., Mezzapesa, D. M., Maria, U., D'Errico, E., Fraddosio, A., & Simone, I. L. (2022). Medulla oblongata volume as a promising predictor of survival in amyotrophic lateral sclerosis. *NeuroImage. Clinical, 34*, Article 103015. https://doi.org/10.1016/j.nicl.2022.103015

Milella, G., Introna, A., Mezzapesa, D. M., D'Errico, E., Fraddosio, A., Ucci, M., Zoccolella, S., & Simone, I. L. (2023). Clinical Profiles and Patterns of Neurodegeneration in Amyotrophic Lateral Sclerosis: A Cluster-Based Approach Based on MR Imaging Metrics. *AJNR. American Journal of Neuroradiology, 44*(4), 403–409. https://doi.org/10.3174/ajnr.A7823

Miller, R. G., Jackson, C. E., Kasarskis, E. J., England, J. D., Forshew, D., Johnston, W., Kalra, S., Katz, J. S., Mitsumoto, H., Rosenfeld, J., Shoesmith, C., Strong, M. J., Woolley, S. C., & Quality Standards Subcommittee of the American Academy of Neurology. (2009). Practice parameter update: The care of the patient with amyotrophic lateral sclerosis: Drug, nutritional, and respiratory therapies (an evidence-based review): Report of the Quality Standards Subcommittee of the American Academy of Neurology. *Neurology, 73*(15), 1218–1226. https://doi.org/10.1212/WNL.0b013e3181bc0141

Pinkhardt, E. H., van Elst, L. T., Ludolph, A. C., & Kassubek, J. (2006). Amygdala size in amyotrophic lateral sclerosis without dementia: An in vivo study using MRI volumetry. *BMC Neurology, 6*, 48. https://doi.org/10.1186/1471-2377-6-48

R Core Team. (2021). *R: A language and environment for statistical computing*. Vienna, Austria: R Foundation for Statistical Computing. https://www.R-project.org/.

Radua, J., Vieta, E., Shinohara, R., Kochunov, P., Quidé, Y., Green, M. J., Weickert, C. S., Weickert, T., Bruggemann, J., Kircher, T., Nenadić, I., Cairns, M. J., Seal, M., Schall, U., Henskens, F., Fullerton, J. M., Mowry, B., Pantelis, C., Lenroot, R., & ENIGMA Consortium collaborators. (2020). Increased power by harmonizing structural MRI site differences with the ComBat batch adjustment method in ENIGMA. *NeuroImage, 218*, Article 116956. https://doi.org/10.1016/j.neuroimage.2020.116956

Rajagopalan, V., Chaitanya, K. G., & Pioro, E. P. (2023). Quantitative Brain MRI Metrics Distinguish Four Different ALS Phenotypes: A Machine Learning Based Study. *Diagnostics (Basel, Switzerland), 13*(9), 1521. https://doi.org/10.3390/diagnostics13091521

Salmanpour, M. R., Bakhtiyari, M., Hosseinzadeh, M., Maghsudi, M., Yousefirizi, F., Ghaemi, M. M., & Rahmim, A. (2023). Application of novel hybrid machine learning systems and radiomics features for non-motor outcome prediction in Parkinson's disease. *Physics in Medicine & Biology, 68*(3), Article 035004. https://doi.org/10.1088/1361-6560/acaba6

Salvatore, C., Castiglioni, I., & Cerasa, A. (2019). Radiomics approach in the neurodegenerative brain. *Aging Clinical and Experimental Research*. https://doi.org/10.1007/s40520-019-01299-z

Schito, P., Ceccardi, G., Calvo, A., Falzone, Y. M., Moglia, C., Lunetta, C., … Filippi, M. (2020). Clinical features and outcomes of the flail arm and flail leg and pure lower motor neuron MND variants: A multicentre Italian study. *Journal of Neurology, Neurosurgery, and Psychiatry, 91*(9), 1001–1003. https://doi.org/10.1136/jnnp-2020-323542

Schuster, C., Hardiman, O., & Bede, P. (2016). Development of an Automated MRI-Based Diagnostic Protocol for Amyotrophic Lateral Sclerosis Using Disease-Specific Pathognomonic Features: A Quantitative Disease-State Classification Study. *PloS One, 11*(12), e0167331.

Schuster, C., Kasper, E., Machts, J., Bittner, D., Kaufmann, J., Benecke, R., Teipel, S., Vielhaber, S., & Prudlo, J. (2014). Longitudinal course of cortical thickness decline in amyotrophic lateral sclerosis. *Journal of Neurology, 261*(10), 1871–1880. https://doi.org/10.1007/s00415-014-7426-4

Smith, S. M., Jenkinson, M., Woolrich, M. W., Beckmann, C. F., Behrens, T. E. J., Johansen-Berg, H., Bannister, P. R., De Luca, M., Drobnjak, I., Flitney, D. E., Niazy, R. K., Saunders, J., Vickers, J., Zhang, Y., De Stefano, N., Brady, J. M., & Matthews, P. M. (2004). Advances in functional and structural MR image analysis and implementation as FSL. *NeuroImage, 23*(Suppl 1), S208–S219. https://doi.org/10.1016/j.neuroimage.2004.07.051

Strong, M. J., Abrahams, S., Goldstein, L. H., Woolley, S., Mclaughlin, P., Snowden, J., Mioshi, E., Roberts-South, A., Benatar, M., HortobáGyi, T., Rosenfeld, J., Silani, V., Ince, P. G., & Turner, M. R. (2017). Amyotrophic lateral sclerosis - frontotemporal spectrum disorder (ALS-FTSD): Revised diagnostic criteria. *Amyotrophic Lateral Sclerosis & Frontotemporal Degeneration, 18*(3–4), 153–174. https://doi.org/10.1080/21678421.2016.1267768

Tafuri, B., Filardi, M., Urso, D., De Blasi, R., Rizzo, G., Nigro, S., & Logroscino, G. (2022). Radiomics Model for Frontotemporal Dementia Diagnosis Using T1-Weighted MRI. *Frontiers in Neuroscience, 16*, Article 828029. https://doi.org/10.3389/fnins.2022.828029

Tafuri, B., Filardi, M., Urso, D., Gnoni, V., De Blasi, R., Nigro, S., Logroscino, G., & Initiative, F. L. D. N. (2023). Asymmetry of radiomics features in the white matter of patients with primary progressive aphasia. *Frontiers in Aging Neuroscience, 15*, 1120935. https://doi.org/10.3389/fnagi.2023.1120935

Tafuri, B., Lombardi, A., Nigro, S., Urso, D., Monaco, A., Pantaleo, E., Diacono, D., De Blasi, R., Bellotti, R., Tangaro, S., & Logroscino, G. (2022). The impact of harmonization on radiomic features in Parkinson's disease and healthy controls: A multicenter study. *Frontiers in Neuroscience, 16*, 1012287. https://doi.org/10.3389/fnins.2022.1012287

Take Action for the Sustainable Development Goals—United Nations Sustainable Development. (n.d.). Retrieved November 9, 2023, from https://www.un.org/sustainabledevelopment/sustainable-development-goals/.

Tan, H. H. G., Westeneng, H.-J., Nitert, A. D., van Veenhuijzen, K., Meier, J. M., van der Burgh, H. K., van Zandvoort, M. J. E., van Es, M. A., Veldink, J. H., & van den Berg, L. H. (2022). MRI Clustering Reveals Three ALS Subtypes With Unique Neurodegeneration Patterns. *Annals of Neurology, 92*(6), 1030–1045. https://doi.org/10.1002/ana.26488

Thome, J., Steinbach, R., Grosskreutz, J., Durstewitz, D., & Koppe, G. (2022). Classification of amyotrophic lateral sclerosis by brain volume, connectivity, and network dynamics. *Human Brain Mapping, 43*(2), 681–699. https://doi.org/10.1002/hbm.25679

Tibshirani, R. (1996). Regression Shrinkage and Selection via the Lasso. *Journal of the Royal Statistical Society. Series B (Methodological), 58*(1), 267–288.

Transforming our world: The 2030 Agenda for Sustainable Development | Department of Economic and Social Affairs. (n.d.). Retrieved November 9, 2023, from https://sdgs.un.org/2030agenda.

van Griethuysen, J. J. M., Fedorov, A., Parmar, C., Hosny, A., Aucoin, N., Narayan, V., Beets-Tan, R. G. H., Fillion-Robin, J.-C., Pieper, S., & Aerts, H. J. W. L. (2017).

Computational Radiomics System to Decode the Radiographic Phenotype. *Cancer Research, 77*(21), e104–e107. https://doi.org/10.1158/0008-5472.CAN-17-0339

Weiner, M. W., Veitch, D. P., Aisen, P. S., Beckett, L. A., Cairns, N. J., Green, R. C., Harvey, D., Jack, C. R., Jagust, W., Morris, J. C., Petersen, R. C., Salazar, J., Saykin, A. J., Shaw, L. M., Toga, A. W., Trojanowski, J. Q., & Alzheimer's Disease Neuroimaging Initiative.. (2017). The Alzheimer's Disease Neuroimaging Initiative 3: Continued innovation for clinical trial improvement. *Alzheimer's & Dementia: The Journal of the Alzheimer's Association, 13*(5), 561–571. https://doi.org/10.1016/j.jalz.2016.10.006

Welsh, R. C., Jelsone-Swain, L. M., & Foerster, B. R. (2013). The utility of independent component analysis and machine learning in the identification of the amyotrophic lateral sclerosis diseased brain. *Frontiers in Human Neuroscience, 7*, 251. https://doi.org/10.3389/fnhum.2013.00251

Wong, T.-T. (2017). Parametric methods for comparing the performance of two classification algorithms evaluated by k-fold cross validation on multiple data sets. *Pattern Recognition, 65*, 97–107. https://doi.org/10.1016/j.patcog.2016.12.018

Zhu, X., Dong, D., Chen, Z., Fang, M., Zhang, L., Song, J., Yu, D., Zang, Y., Liu, Z., Shi, J., & Tian, J. (2018). Radiomic signature as a diagnostic factor for histologic subtype classification of non-small cell lung cancer. *European Radiology, 28*(7), 2772–2778. https://doi.org/10.1007/s00330-017-5221-1

Zoccolella, S., Mastronardi, A., Scarafino, A., Iliceto, G., D'Errico, E., Fraddosio, A., Tempesta, I., Morea, A., Scaglione, G., Introna, A., & Simone, I. L. (2020). Motor-evoked potentials in amyotrophic lateral sclerosis: Potential implications in detecting subclinical UMN involvement in lower motor neuron phenotype. *Journal of Neurology, 267*(12), 3689–3695. https://doi.org/10.1007/s00415-020-10073-5

Zwanenburg, A., Leger, S., Vallières, M., & Löck, S. (2020). Image biomarker standardisation initiative. *Radiology, 295*(2), 328–338. https://doi.org/10.1148/radiol.2020191145